ROYAL SOCIETY
OF CHEMISTRY

## COMMUNICATION

# Quantitative evaluation of accelerated transdermal drug delivery by electroosmosis *via* frustoconical porous microneedles†

Soichiro Tottori,[a] Sae Ichinose,[a] Fumika Sakai,[a] Reiji Segawa,[b] Taiki Yokoyama,[a] Gaobo Wang[a] and Matsuhiko Nishizawa ⭐[abc]

Electroosmosis-based transdermal drug delivery *via* frustoconical porous microneedles (F-PMNs) is studied by quantitative fluorescence analysis of the drug models penetrated into excised pig skin. An array of 300 μm height F-PMN made of poly-glycidyl methacrylate is modified by a grafted thin film of anionic poly (2-acrylamido-2-methylpropanesulfonic acid) (PAMPS) or a cationic poly-(3-acrylamidopropyl trimethylammonium) (PAPTAC) to generate electroosmotic flow (EOF) upon application of current through the needles. Owing to the synergy of the EOF-promoted transport and the expansion of the stratum corneum with the frustoconical protrusions, the penetration rates of rhodamine B (479 Da) and FITC-dextran (4 kDa and 10 kDa) are found to be accelerated by more than 10 times. In addition, the F-PMNs modified with PAMPS and PAPTAC show similar delivery rates in opposite directions, enabling the possible dual-mode delivery from both anode and cathode in an integrated iontophoresis device.

## Introduction

Transdermal drug delivery has been attracting attention to avoid several inconveniences of oral medication such as the hepatic first-pass effect, gastric pH-induced hydrolysis, and unpleasant side effects of drugs.[1–3] Microneedles (MNs) have become a promising platform for the transdermal delivery that is painless, less invasive, and easy to self-administer. In addition to the progress in conventional homogeneous solid MNs,[4–6] solid-based porous microneedles (PMNs)[7–14] have

recently been developed as a new type of MN which has a micro/nanochannel network throughout the whole needle, thereby providing a route for the transdermal administration of drugs. Also, PMNs can serve as a tank of drug solution that can be continuously delivered. In addition, since the PMNs can pass ionic currents, iontophoresis[15–20] has been conducted *via* PMNs to enhance the transdermal dosing of drugs and the extraction of biomarkers by mainly utilizing electrophoretic movement of molecules. Importantly, the charge-immobilized PMNs can generate larger electroosmotic flow (EOF),[21–24] which dominates the molecular transport (even in the reverse direction of electrophoresis) regardless of their charge. Recently, a novel PMN device with bilaterally aligned EOF for controllable dual-mode delivery of molecules has been realized by using the anionic and cationic PMNs for anode and cathode compartments.[25]

On the other hand, the application of EOF through the non-invasive frustoconical PMN (F-PMN) has been recently reported to allow penetration of larger (over 500 Da) molecules, such as dextran (∼10 kDa), into skin.[26] However, the discussion has been limited to quantitative phenomena based on fluorescent images of cross-sectioned skin after the delivery experiments. Therefore, in the present study, the performance of EOF-based transdermal drug delivery *via* F-PMNs (Fig. 1) is evaluated by quantitative fluorescent analysis of the molecules delivered into skin. In addition to the anionic modification, the cationic polymer-modified PMNs are studied to quantitatively examine the possible dual-mode delivery from both the anode and cathode in the minimally invasive iontophoresis.

## Results and discussion

The array of frustoconical porous microneedles (F-PMN) made up of aggregated particles of poly-glycidyl methacrylate was prepared by molding (Fig. S1, ESI†) as described in the previous paper.[25,26] The F-PMN has internal porous structures (porosity, *ca.* 45%) with

[a] *Department of Finemechanics, Graduate School of Engineering, Tohoku University, 6-6-1 Aramaki Aoba, Aoba-ku, Sendai 980-8579, Japan.*
*E-mail: nishizawa@tohoku.ac.jp*
[b] *Department of Biomedical Engineering, Graduate School of Biomedical Engineering, Tohoku University, 6-6-4 Aramaki Aoba, Aoba-ku, Sendai 980-8579, Japan*
[c] *bionto Co., Material Innovation Center, Tohoku University, 468-1 Aramaki Aoba, Aoba-ku, Sendai, 980-8579, Japan*

This journal is © The Royal Society of Chemistry 2025
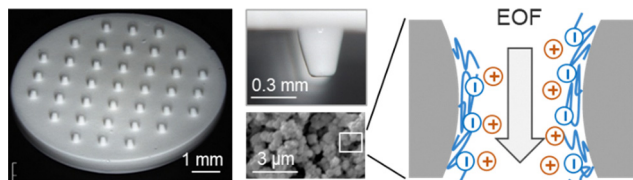
*J. Mater. Chem. B*, 2025, **13**, 5023–5026 | **5023**

Fig. 1 Images of the F-PMN (an array of 37 needles of 300 μm height; 45% porosity), and the illustration of the electroosmotic flow (EOF) generated in the direction of the movement of cations *via* the anionic polymer-modified PMN.

interconnecting pores of *ca.* 1.0 μm diameter on average. The substrate of the F-PMN array chip was 8 mm in diameter; the surface area was 0.5 cm$^2$. By using the setup illustrated in Fig. 2a, the transdermal electrical DC resistance was measured *via* a pair of F-PMNs indented to the skin of subject's arm, in accordance with the standards of Ethics Committee of Graduate School of Engineering, Tohoku University (23A-14). Ag/AgCl electrodes were connected to the F-PMNs through the tubular salt bridges, and a current of 1 μA was applied by a current source. The resistance of the F-PMN filled with PBS solution was ~0.5 kΩ. As shown in Fig. 2b, the intact skin without the F-PMNs showed significantly larger and scattered resistance in the range of MΩ due to the insulating nature of the stratum corneum (SC).[27] Comparatively, the use of F-PMNs with heights of 300, 600, or 800 μm resulted in a reduction and stabilization of trans-dermal resistance to 100–300 kΩ. Trypan Blue staining
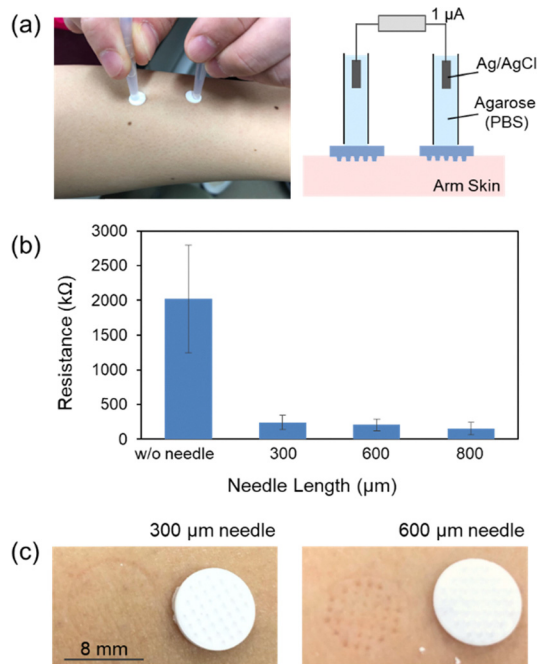


Fig. 2 Expansion of stratum corneum with the frustoconical protrusions. (a) Setup for measuring transdermal DC resistance through F-PMNs indented to the skin of subject's arm. (b) Average resistance values at *ca.* 15 N for F-PMNs of different lengths (300, 600, 800 μm) (*n* = 4 independent experiments; mean ± SD). (c) Typical photographs of the arm skin immediately after the resistance measurements.

indicated that the cell membrane of SC keratocytes were not ruptured (Fig. S2, ESI†). Therefore, it can be concluded that the SC was not broken but only deformed by the F-PMNs. The permeabilization of the skin by expanded deformation of the SC is of interest from the viewpoint of minimally invasive transdermal delivery. Although a lower resistance was observed with longer needles, the 300 μm-height F-PMNs were selected in the following experiments because the longer 600 μm F-PMN left tracks of deformation as shown in Fig. 2c.

The transdermal delivery of model drugs, rhodamine B (RB) and FITC-dextran, into pig skin was conducted using the setup illustrated in Fig. 3a with an anionic PAMPS-modified F-PMN (300 μm height). The F-PMNs were immersed in a PBS solution of model drugs (0.5 mg ml$^{-1}$ for RB, 5 mg ml$^{-1}$ for dextrans) for overnight for pre-loading into the pore of F-PMNs. The F-PMN and the plate were pressed onto the pig skin with a force of 15 N, followed by connecting to a current source *via* agarose salt bridges and Ag/AgCl electrodes. As conceptually illustrated in Fig. 3b, the non-penetrating charge-immobilized F-PMN is expected to accelerate the transdermal drug delivery by the synergy of expansion of stratum corneum and the active transport by EOF. The skin area under the F-PMN (*ca.* 10 mm × 10 mm) was excised, digested with proteinase K, and centrifuged for fluorescence intensity measurement (Fig. 3c). The amount of excised porcine skin did not significantly affect the fluorescence measurement, as confirmed in the process of creating a calibration curve for 10 kDa dextran (Fig. S3, ESI†).

The amount of RB penetrated into the skin was found to linearly increase during the application of 0.5 mA cm$^{-2}$ (or 0 mA cm$^{-2}$) for 40, 80, and 120 min, as shown in Fig. 3d. The current strength of 0.5 mA cm$^{-2}$ is usually considered to be the maximal current density for safety reasons.[28] A quantitative comparison of the penetration rates (the slopes of the plots) of RB between the cases of the flat plate (0.5 mA cm$^{-2}$), the F-PMN (0 mA cm$^{-2}$), and the F-PMN (0.5 mA cm$^{-2}$). A significant enhancement in the penetration rate was examined for the effects of the expansion of SC with F-PMN (×5) and of the generation of EOF (×12). The average penetration rate of RB through PAMPS-modified F-PMN was 48 ng min$^{-1}$, corresponding to *ca.* 96% transportation efficiency calculated using the EOF rate of *ca.* 0.1 μL min$^{-1}$,[22] generated through pig skin; the concentration of RB solution penetrated into skin was nearly the same as original solution loaded in the F-PMN. This result indicates that the barrier of SC for RB (479 Da) transportation becomes negligible by the expansion effect of F-PMN.

The dosing of larger model drugs (>500 Da), specifically dextran (4 kDa and 10 kDa), was studied next using the PAMPS-modified F-PMNs (300 μm height). Fig. 3e shows the amount of dextran penetrated into the skin with and without the application of 0.5 mA cm$^{-2}$ for 40, 80, and 120 min. The passive penetration of both dextrans at 0 mA cm$^{-2}$ through the skin deformed by F-PMNs was less than 1 μg even after 120 min. In contrast, the penetration was significantly enhanced by applying EOF. The penetration rates of 4 kDa dextran and 10 kDa dextran were accelerated *ca.* 14 times and *ca.* 24 times, respectively, by applications of EOF. Because dextran penetration was
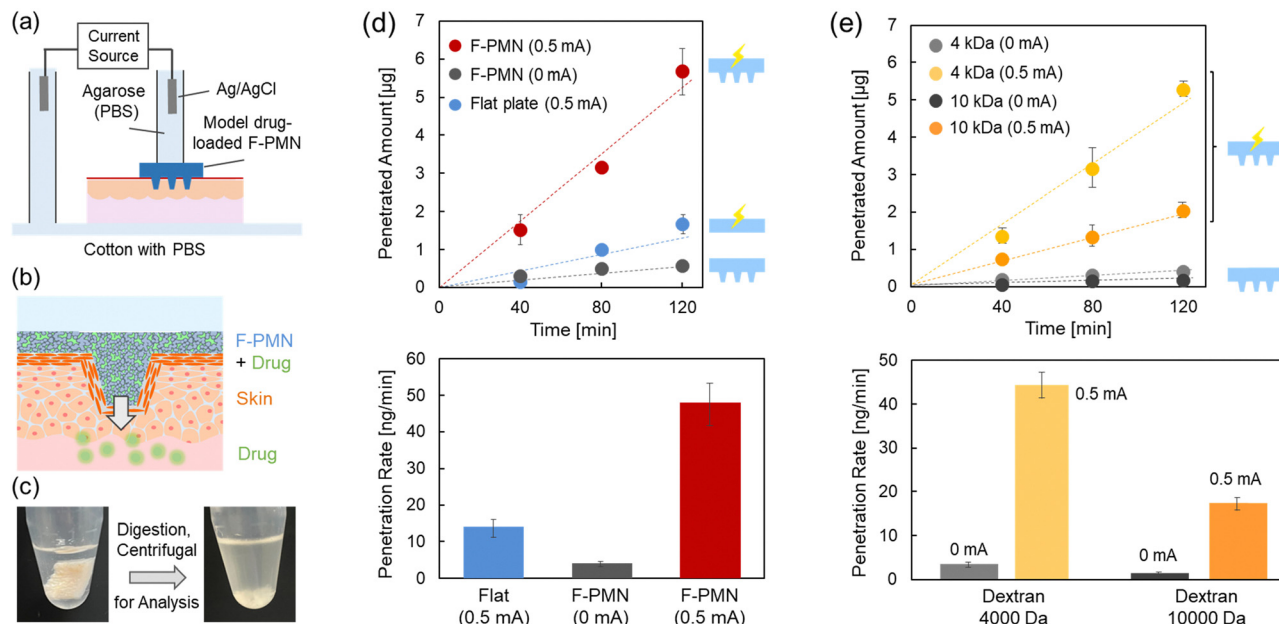
5024 | *J. Mater. Chem. B*, 2025, **13**, 5023–5026

This journal is © The Royal Society of Chemistry 2025

**Fig. 3** Electroosmosis-promoted transdermal delivery through anionic polymer-modified F-PMN. (a) Schematic of the setup for the EOF-promoted drug delivery to pig skin. (b) Conceptual illustration of the EOF-promoted transdermal drug delivery *via* the non-penetrating charge-immobilized F-PMN, highlighting the synergy of the expansion of stratum corneum and the active transport by EOF. (c) The skin under the F-PMN was excised, enzymatically digested, and evaluated by fluorescent measurements. (d) The amount of RB penetrated into the skin by application of 0.5 mA cm$^{-2}$ (or 0 mA cm$^{-2}$) to the F-PMNs and a flat porous plate for 40, 80 and 120 min. The penetration rate of RB for the flat plate (0.5 mA cm$^{-2}$), the F-PMN (0 mA cm$^{-2}$) and the F-PMN (0.5 mA cm$^{-2}$). $N$ = 3 independent experiments; mean ± SD. (e) The amount of FITC-dextran (4 kDa and 10 kDa) penetrated into the skin by application of 0.5 mA cm$^{-2}$ (or 0 mA cm$^{-2}$) to the F-PMNs for 40, 80 and 120 min. The penetration rate of dextrans from the F-PMN (0 mA cm$^{-2}$ or 0.5 mA cm$^{-2}$). $N$ = 3 independent experiments; mean ± SD.

not observed for the PAMPS-modified porous "flat" substrate even with the application of 0.5 mA cm$^{-2}$ for 120 min,[26] it can be concluded that the combination of (i) the expansion of SC of skin with the frustoconical protrusions of the F-PMN and (ii) the EOF-promoted ejection enables effective transdermal administration of larger molecule such as dextran, whose size is comparable to that of many drugs, including insulin (*ca.* 6000 Da). The transportation efficiency for 4 kDa dextran and 10 kDa dextran were estimated to be *ca.* 9% and *ca.* 4%, indicating the expanded SC still exhibits barrier property to the transport of dextrans. In fact, the use of a sharp PMN, which breaks SC, increased the efficiency for 10 kDa dextran to *ca.* 8% (Fig. S4, ESI†). It can be expected that optimizing the shape and spacing of the F-PMNs and sealing the substrate[12] will improve the transportation efficiency.

The combination of the F-PMNs modified with anionic PAMPS and cationic PAPTAC enables controllable dual-mode delivery of molecules by the bilaterally aligned EOF, as illustrated in Fig. 4a, since the directions of EOF in the anionic and cationic F-PMNs are opposite to each other.[25,29] Fig. 4b shows the amount of 10 kDa dextran penetrated from the PAMPS-modified and PAPTAC-modified F-PMNs into the skin during the application of 0.5 mA cm$^{-2}$ and −0.5 mA cm$^{-2}$ for 40, 80, and 120 min. Because the anionic and cationic modifications were optimized to balance the ejection rates,[25] it was quantitatively proved that the degrees of acceleration in penetration of dextran through the deformed SC were comparable. The combination of these F-PMNs can prevent unwanted cathodal suction
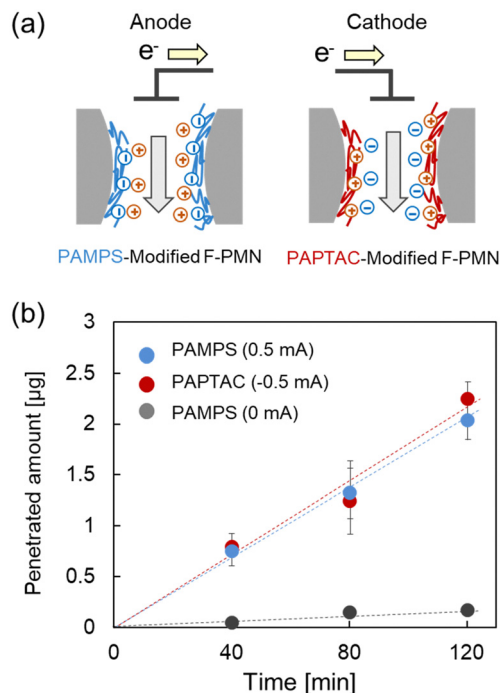


**Fig. 4** Combination of anionic and cationic F-PMNs for dual-mode delivery. (a) Setup for measuring transdermal DC resistance through F-PMNs indented to the skin of subject's arm. (b) Average resistance values at *ca.* 15 N for F-PMNs of different lengths (300, 600, 800 μm) (*n* = 4 independent experiments; mean ± SD). (c) Typical photographs of the arm skin immediately after the resistance measurements.

This journal is © The Royal Society of Chemistry 2025

*J. Mater. Chem. B*, 2025, **13**, 5023–5026 | **5025**

of interstitial fluid and promote the development of a compact iontophoresis system with the integrated anodic and cathodic F-PMNs in closed proximity (Fig. S5, ESI†).

## Conclusions

The significant acceleration of transdermal drug penetration by EOF *via* the F-PMNs was quantitatively confirmed here. The mechanism behind this acceleration is the synergy of expansion of stratum corneum, evidenced by the change in transdermal DC resistance, and the active transport by EOF generated in the F-PMNs. The penetration rate of RB (479 Da) was found to be accelerated by 12 times. Importantly, the penetration of a larger drug model, dextran (∼10 kDa) was made possible by the expansion of stratum corneum, and the rate of penetration was accelerated by 14 times for 4 kDa dextran and 24 times for 10 kDa dextran. The transportation efficiency was unfortunately less than 10% for these dextrans, but it can be improved by optimizing the shape and spacing of F-PMNs. Based on the quantitative examination of the aligned EOF from the anionic and cationic F-PMNs, an integrated device for dual-mode iontophoretic delivery is currently under development.

## Author contributions

M. Nishizawa: conceived and designed the experiments. S. Ichinose, F. Sakai, R. Segawa, and T. Yokoyama: performed experiments. S. Tottori, G. Wang, and M. Nishizawa: analyzed the data and wrote the manuscript. All authors discussed the results and contributed to the final manuscript.

## Data availability

The data supporting this article have been included as part of the ESI.†

## Conflicts of interest

The authors declare no conflict of interest.

## Acknowledgements

## Notes and references

1 M. R. Prausnitz and R. Langer, *Nat. Biotech.*, 2008, **26**, 1261.
2 A. Z. Alkilani, M. T. C. McCrudden and R. F. Donnelly, *Pharmaceutics*, 2015, **7**, 438.
3 W. Y. Jeong, M. Kwon, H. E. Choi and K. S. Kim, *Biomater. Res.*, 2021, **25**, 24.
4 J. H. Jung and S. G. Jin, *J. Pharm. Invest.*, 2021, **51**, 503.
5 S. Pahal, K. Badnikar, V. Ghate, U. Bhutani, M. M. Nayak, D. N. Subramanyam and P. K. Vemul, *Eur. J. Pharm. Biopharm.*, 2021, **159**, 151.
6 W. Li, J. Tang, R. N. Terry, S. Li, A. Brunie, R. L. Callahan, R. K. Noel, C. A. Rodríguez, S. P. Schwendeman and M. R. Prausnitz, *Sci. Adv.*, 2019, **5**, 8145.
7 L. Bao, J. Park, G. Bonfante and B. Kim, *Drug Delivery Transl. Res.*, 2022, **12**, 395.
8 Y. T. He, L. Liang, Q. Zhao, L. F. Hu, W. M. Fei, B. Z. Chen, Y. Cui and X. D. Guo, *J. Drug Delivery Sci. Technol.*, 2022, **74**, 103518.
9 P. J. Vos, N. Kuijt, M. Kaya, S. Rol and K. van der Maaden, *Eur. J. Pharm. Sci.*, 2020, **150**, 105331.
10 L. Liu, H. Kai, K. Nagamine, Y. Ogawa and M. Nishizawa, *RSC Adv.*, 2016, **6**, 48630.
11 K. Nagamine, J. Kubota, H. Kai, Y. Ono and M. Nishizawa, *Biomed. Microdev.*, 2017, **19**, 68.
12 Y. Abe, R. Takizawa, N. Kimura, K. Konno, S. Yoshida and M. Nishizawa, *Biomed. Eng. Adv.*, 2021, **1**, 100004.
13 G. Wang, K. Kato, I. Aoki, S. Ichinose, D. Inoue, S. Tottori and M. Nishizawa, *J. Mater. Chem. B*, 2024, **12**, 1490.
14 E. M. Eltayib, A. Himawan, U. Detamornrat, W. K. Muhtadi, H. Li, L. Li, L. Vora and R. F. Donnelly, *Pharm. Dev. Technol.*, 2024, **29**, 164.
15 N. Dixit, V. Bali, S. Baboota, A. Ahuja and J. Ali, *Curr. Drug Delivery*, 2007, **4**, 1.
16 Y. Li, J. Yang, Y. Zheng, R. Ye, B. Liu, Y. Huang, W. Zhou and L. Jiang, *Acta Biomater.*, 2021, **121**, 349.
17 X. Li, X. Huang, J. Mo, H. Wang, Q. Huang, C. Yang, T. Zhang, H.-J. Chen, T. Hang, F. Liu, L. Jiang, Q. Wu, H. Li, N. Hu and X. Xie, *Adv. Sci.*, 2021, **8**, 2100827.
18 Y. Zheng, R. Ye, X. Gong, J. Yang, B. Liu, Y. Xu, G. Nie, X. Xie and L. Jiang, *Microsyst. Nanoeng.*, 2023, **9**, 35.
19 R. Z. Seeni, M. Zheng, D. C. S. Lio, C. Wiraja, M. F. B. Yusoff, W. T. Y. Koh, Y. Liu, B. T. Goh and C. Xu, *Adv. Funct. Mater.*, 2021, **31**, 2105686.
20 U. Detamornrat, M. Parrilla, J. Domínguez-Robles, Q. K. Anjani, E. Larrañeta, K. De Wael and R. F. Donnelly, *Lab Chip*, 2023, **23**, 2304–2315.
21 M. J. Pikal, *Adv. Drug Delivery Rev.*, 2001, **46**, 281.
22 S. Kusama, K. Sato, Y. Matsui, N. Kimura, H. Abe, S. Yoshida and M. Nishizawa, *Nat. Commun.*, 2021, **12**, 658.
23 H. Abe, K. Sato, K. Kimura, S. Kusama, D. Inoue, K. Yamasaki and M. Nishizawa, *Adv. NanoBiomed. Res.*, 2022, **2**, 2100066.
24 H. Terui, N. Kimura, R. Segawa, S. Kusama, H. Abe, D. Terutsuki, K. Yamasaki and M. Nishizawa, *J. Drug Delivery Sci. Technol.*, 2022, **75**, 103711.
25 G. Wang, K. Kato, S. Ichinose, D. Inoue, A. Kobayashi, H. Terui, S. Tottori, M. Kanzaki and M. Nishizawa, *Adv. Healthcare Mater.*, 2024, **13**, 2401181.
26 D. Terutsuki, R. Segawa, S. Kusama, H. Abe and M. Nishizawa, *J. Controlled Release*, 2023, **354**, 694.
27 Y. Abe and M. Nishizawa, *APL Bioeng.*, 2021, **5**, 041509.
28 M. Roustit, S. Blaise and J. L. Cracowski, *Br. J. Clin. Pharmacol.*, 2013, **77**, 63.
29 D. Terutsuki, S. Miyazawa, J. Takagi, A. Yamada, Y. Sun, H. Abe, G. Wang and M. Nishizawa, *Adv. Funct. Mater.*, 2023, **34**, 2304946.

5026 | *J. Mater. Chem. B*, 2025, **13**, 5023–5026

This journal is © The Royal Society of Chemistry 2025